Transition rates, branching ratio, and lifetime of the $2p^3 3s\ {}^5S^\circ_2$ metastable state in O I

Xueyang Zhang [1,2] Xiaozhi Shen [2,3,*] Ping Yuan [1,†] and Feng Hu [4]

[1] *Key Laboratory of Atomic and Molecular Physics and Functional Materials of Gan Su Province, College of Physics and Electronic Engineering, Northwest Normal University, Lanzhou 730070, China*

[2] *School of Mechatronical Engineering, Handan University, Handan 056005, China*

[3] *School of Science and Engineering in Mathematics and Physics, Hebei University of Engineering, Handan 056038, China*

[4] *School of Physics and New Energy, Xuzhou University of Technology, Xuzhou 221018, China*

(Received 25 March 2020; revised 9 September 2020; accepted 9 September 2020; published 30 October 2020)

Based on the multiconfiguration Dirac-Hartree-Fock method, the accurate line strengths, transition rates, branching ratio, branching fraction, and lifetime of the $2p^3 3s\ {}^5S^\circ_2$ metastable state of neutral oxygen atom (O I), together with the uncertainties evaluated from the residual electron correlation effects, are determined by taking into account the effects of core-core, core-valence, and valence correlations, the Breit interaction, and QED effect. It is shown that the core correlation effect has a certain influence if the separation between ${}^3S^\circ$ and ${}^5S^\circ$ in the $p^3 s$ configuration is accurately calculated. It is found that the calculations of branching ratio of ${}^5S^\circ_2$ remain stable in different electron correlation models. We infer that it is a peculiar intrinsic property leading to results useful for plasma diagnostics and other applications. The transition rates from ${}^5S^\circ_2$ change considerably as a result of the Breit interaction, because the line strengths of ${}^3P_2$–${}^5S^\circ_2$ (λ135.560 nm) and ${}^3P_1$–${}^5S^\circ_2$ (λ135.851 nm) are different in sensitivity to this effect. This affects the calculations of the branching ratio and lifetime. There exist large discrepancies among several calculations of lifetimes, such as the MCHF calculation by [C. Froese Fischer and G. Tachiev, At. Data Nucl. Data Tables **87**, 1 (2004)]. The main reasons are ascribed to the neglected electron correlation and relativistic effects. In addition, by checking different calculations with various sets of multireference configurations, we find that the calculations of the electric dipole matrix elements for ${}^5S^\circ_2$ in the length gauge are much more sensitive to electron correlation effects than in the velocity gauge. This may also lead to some errors in the calculations of the lifetime of ${}^5S^\circ_2$ in the length gauge.

DOI: 10.1103/PhysRevA.102.042824

I. INTRODUCTION

The electronically excited states of atoms and molecules for which the electric dipole matrix element for transitions to all lower states is zero or very small are known as metastable states [1]. An example is the ${}^5S^\circ_2$ level in the $p^3 s$ configuration. The atomic data for ${}^5S^\circ_2$ in the carbonlike isoelectronic sequence are often used to diagnose the astrophysical plasma [2,3]. The radiative decay rates from ${}^5S^\circ_2$ in C I were evaluated by Haris and Kramida through comparison of some experimental data with theoretical and semiempirical results [3]. Rubin *et al.* also adopted the rates from ${}^5S^\circ_2$ in N II to estimate the electron density and temperature of the Orion nebula using the Goddard high-resolution spectrograph and the faint object spectrograph on the Hubble space telescope [2]. These motivate us to evaluate whether the ${}^5S^\circ_2$ level of O I has the properties that are similar to those of C I or N II.

Many celestial bodies in the universe are rich in oxygen. From 2015 to 2020, the atomic data of ${}^5S^\circ_2$ in O I were widely applied in the determination of the ionospheric properties of atmosphere and astrophysical diagnosis [4–9]. For example, the atomic data for remote sensing at 135.6 nm with the radiative channel $2p^4\ {}^3P_2$–$2p^3 3s\ {}^5S^\circ_2$ in the night time ionosphere were used to estimate the ionospheric electron density by Qin *et al.* [5]. They adopted Meier's calculated data based on the *gf* values of Zeippen *et al.* [10,11]. The line mentioned above is strongly correlated with the line at 130.4 nm arising from the transition $2p^4\ {}^3P_1$–$2p^3 3s\ {}^3S^\circ_1$ [12], and their intensity ratio λ135.6/130.4 nm varies due to some differences in the atmospheric composition, for example, between Ganymede's leading and trailing hemispheres [13]. The ratio λ135.6/130.4 nm was also used to determine the oxygen content in gases; e.g., Feldman *et al.* suggested that the main source of gas outbursts on the comet 67P is oxygen [14], and Roth *et al.* confirmed that the atmosphere of Europa is dominated by O_2 [15]. There exist some works about the application of the 135.6-nm line, just reported in 2020, such as the first synoptic observations of geomagnetic storm effects [8] and the derivation of global O/N_2 ratios [9].

For a complex $n_1 p^3 n_2 s$ ($n_1 \leqslant n_2$) configuration, the *p*-*p* electron interaction produces three terms—$({}^2P^\circ)$, $({}^2D^\circ)$, and $({}^4S^\circ)$—of a p^3 configuration under good *LS* coupling condition [16]. Six Rydberg series of levels with different multiplicities and *L* values of the final *LS* terms are produced: $n_1 p^3({}^2P^\circ) n_2 s\ {}^1P^\circ$ and ${}^3P^\circ$, $n_1 p^3({}^2D^\circ) n_2 s\ {}^1D^\circ$ and ${}^3D^\circ$, $n_1 p^3({}^4S^\circ) n_2 s\ {}^3S^\circ$ and ${}^5S^\circ$. Once n_2 increases and is greater than n_1, the *s*-electron moves far from the core, so that the *p*-*s* interaction decreases [16]. In this case, the Coulomb separation between $({}^4S^\circ)\,{}^3S^\circ$ and $({}^4S^\circ)\,{}^5S^\circ$ becomes much narrower. For example, the separation is 108 342 cm^{-1} in the $2p^3 2s$

*shenxz@buaa.edu.cn

†yuanp@nwnu.edu.cn

(a.k.a. $2s2p^3$) configuration of N II, whereas it decreases to 3027 cm^{-1} in $2p^3 3s$ of O I, with a change of approximately 36 times [17]. Thus, it is interesting to compare the splitting between terms based on $p^3(^4S^\circ)$ in different situations, which can help researchers understand the physical laws of complex atomic systems. For instance, it is necessary to know what different schemes should be used in the calculations, when the core correlation effect or relativistic effect is considered or not. This information can be used to guide the actual high-precision calculations.

The effect of electron correlations, including that of the innermost $1s^2$ electrons, on the energies of the p^3s configuration is larger than for other configurations. Shen *et al.* presented the example of the energies of $2p^3 2s$ (or $2s2p^3$) in the N II ions [18]. It was shown that the CC and CV correlation effects change the excitation energy of the $2p^3(^4S^\circ)2s\ ^3S^\circ$ level of N II by approximately 1187 cm^{-1}, which is almost three times larger than the changes in the energies of other configurations [18]. Whether the core correlation effect influences the energy of the $p^3 s$ configuration in O I needs to be determined.

The transition rates from the $^5S^\circ_2$ level in O I are very sensitive to electron correlation effects and other corrections due to their very small values of approximately $10^3\ s^{-1}$ (similar to that of $^5S^\circ_2$ in N II). Accurate calculation of the very small transition matrix elements is quite challenging. Few studies on the core correlation effect have been performed in the past [11,19–23]. Shen *et al.* mentioned that the effects of CC and CV correlation influence the rates from $^5S^\circ_2$ in N II with different convergence speeds [24]. The influence of electron correlations arising from the electrons in the deep subshells, even on the energy levels of livermorium (nuclear charge $Z = 116$), is also obvious [25]. In addition, some important valence correlations must be involved adequately. For example, Hibbert pointed out that the intercombination transitions from $^5S^\circ_2$ in N II are critically dependent on the accuracy of the mixing between the upper $2s2p^3\ ^5S^\circ_2$ level and the $2s2p^3\ ^3P^\circ_2$, $^3D^\circ_2$ levels, as well as $2s^2 2p3s\ ^3P^\circ_2$ and $2s^2 2p3d\ ^3P^\circ_2$, all of which allow a contribution to the dipole operator for transitions to the ground-state levels [26]. Furthermore, the relativistic correction in the low-frequency limit of the transverse photon interaction, namely, the Breit interaction, also has a large influence on the rates from $^5S^\circ_2$ in N II. This causes a large effect in the corresponding calculations of the branching ratio [24]. This influence is the second-most important for the rates from $^5S^\circ_2$ in N II, following the electron correlation effect [24]. These findings require us to perform detailed studies on the transition rates from $^5S^\circ_2$ in O I.

When diagnosing astrophysical media, researchers are very interested in the radiative lifetime of $^5S^\circ_2$ in O I, because its value is considerably large, 180 ± 5 μs [27,28]. A common method of observation is the time-of-flight (TOF) technique, which considers an atomic beam to be a diffuse gas source with a known velocity distribution. Using this method, Johnson [29], Wells and Zipf [30], Nowak *et al.* [31], and Mason [1] successively measured the lifetime of $^5S^\circ_2$. Wiese *et al.* averaged their four lifetimes to obtain 180 ± 5 μs [27,28] that can be recommended in the applications. For example, using the values of branching ratio of $^5S^\circ_2$ [11], the transition rates $A(^3P_2–^5S^\circ_2)$ and $A(^3P_1–^5S^\circ_2)$ could be derived from the accurately known recommended lifetime [27].

It must be stressed that large discrepancies were met in several theoretical calculations of lifetimes. In contrast to two calculations with the reported lifetimes of about 200 μs [20,21], Froese Fischer's MCHF calculations in the length gauge gave a value of approximately 560 μs, although her calculations were repeated twice [22,23]. Garstang's calculation also yielded a value of nearly 600 μs [19]. However, a very small value of 129 μs was reported by Zeippen *et al.* [11]. These large discrepancies, within the range of 129–591 μs, may be ascribed to deficiencies in calculations, e.g., the core correlation effect is rarely considered [11,19–23], the calculations of transition matrix elements present some differences in the length and velocity gauges for extremely weak decays [11,20], some neglected relativistic effects may affect the accuracy of calculations (e.g., Breit interaction), etc. One of the purposes of the present work is to investigate possible ways to overcome these difficulties.

II. THEORETICAL METHOD AND COMPUTATIONAL MODELS

A. Theoretical method

The atomic state wave functions (ASFs) can be generated using the MCDHF method [32,33]. The ASFs are linear combinations of configuration state functions (CSFs) with the same parity P and angular momentum J,

$$\Psi(\Gamma PJ) = \sum_{j=1}^{n_c} c_j \Phi(\gamma_j PJ), \tag{1}$$

where n_c is the number of CSFs. c_j and γ_j are, respectively, the mixing coefficient and other appropriate labeling of the CSFs built from products of one-electron Dirac orbitals. The self-consistent field (SCF) method was employed to optimize the radial parts of the Dirac orbitals and the expansion coefficients, and an extended optimal level (EOL) scheme was further applied to obtain balanced energies for the studied states. The Hamiltonian operator of the Breit interaction [34] is given as

$$\hat{H}^{\text{Breit}}(ij) = -\frac{1}{2r_{ij}}\left[\vec{\alpha}_i \cdot \vec{\alpha}_j + \frac{(\vec{\alpha}_i \cdot \vec{r}_{ij})(\vec{\alpha}_j \cdot \vec{r}_{ij})}{r_{ij}^2}\right], \tag{2}$$

where α_i is the Dirac matrix of the i^{th} electron, and $\vec{r}_{ij} = \vec{r}_i - \vec{r}_j$ denotes the distance between a pair of electrons i and j. The quantum electrodynamics (QED) effects, including self-energy and vacuum polarization, were included in subsequent relativistic configuration interaction (RCI) calculations [32].

The electric dipole transition rate from an upper state u to a lower one l can be written [35] as

$$A = \frac{4}{3}\alpha \frac{(E_u - E_l)^3}{\hbar^3 c^2} \frac{S}{2J_u + 1}, \tag{3}$$

where α and $E_u - E_l$ (or ω) are, respectively, the fine structure constant and transition energy. $\hbar$, c, and J_u represent the Planck constant, speed of light, and the total angular momentum of the upper level. S is the line strength, which can be defined by the square of reduced nondiagonal matrix element

TABLE I. The computational models including those of CASE-I, II, III, and the higher-order correlation. DHF, *n*SDV ($n = 4, ..., 8$), CV, CC&CV, Breit, and QED, respectively, stand for the single configuration calculation, valence (V), core-valence (CV), combined CC and CV (CC&CV), Breit interaction, and QED effect. The CASE-I is the main calculation for studying the physical properties. CASE-II and III are used for estimations of the set of multireference configurations (SMC). TQ denotes triple and quadruple (TQ) substitutions. 4–44 173 show the variation range of the number of CSFs from the DHF model to the 7SDV model.

Reference configurations				Number of CSFs		
Odd	Even	Models	Active spaces	$J = 2$(odd)	$J = 1$(even)	$J = 2$(even)
		CASE-I (Main part for studying physical property)				
$\{2s^2\,2p^3 3s\}$	$\{2s^2 2p^4\}$	DHF	$n = 2-3, l = \mathrm{s-p}$	4	1	2
		4SDV	$n = 2-4, l = \mathrm{s-f}$	3542	1267	1658
		5SDV	$n = 2-5, l = \mathrm{s-g}$	10 931	3581	4901
		6SDV	$n = 2-6, l = \mathrm{s-h}$	24 619	7631	10 817
		7SDV	$n = 2-7, l = \mathrm{s-h}$	44 173	13 355	19 207
		8SDV	$n = 2-8, l = \mathrm{s-h}$	69 593	20 753	30 071
$\{1s^2 2s^2\,2p^3 3s\}$	$\{1s^2 2s^2 2p^4\}$	CV	$n = 1-8, l = \mathrm{s-h}$	173 916	49 814	71 814
$\{1s^2 2s^2\,2p^3 3s\}$	$\{1s^2 2s^2 2p^4\}$	CC&CV, Breit	$n = 1-8, l = \mathrm{s-h}$	190 454	54 334	78 434
$\{1s^2 2s^2\,2p^3 3s\}$	$\{1s^2 2s^2 2p^4\}$	QED	$n = 1-8, l = \mathrm{s-h}$	190 454	54 334	78 434
		CASE-II (Estimation of SMC)				
$\{2s^2\,2p^3 3s\}$	$\{2s^2 2p^4\}$	DHF–*n*SDV	$n = 2-7, l = \mathrm{s-h}$	4 – 44 173	1 – 13 355	2 – 19 207
$\{1s^2 2s^2\,2p^3 3s,\ 1s^2 2s^2 2p^3 3d\}$	$\{1s^2 2s^2 2p^4,\ 1s^2 2s^2 2p^3 3p\}$	CC&CV, Breit	$n = 1$–$7, l = \mathrm{s-h}$	488 154	214 617	309 315
		CASE-III (Estimation of SMC)				
$\{2s^2 2p^3 3s,\ 2s^2 2p^3 3d\}$	$\{2s^2 2p^4,\ 2s^2 2p^3 3p\}$	DHF–*n*SDV	$n = 2$–$7, l = \mathrm{s-i}$	14 – 166 866	10 – 71 914	11 – 104 655
$\{1s^2 2s^2\,2p^3 3s,\ 1s^2 2s^2 2p^3 3d\}$	$\{1s^2 2s^2 2p^4,\ 1s^2 2s^2 2p^3 3p\}$	CC&CV, Breit	$n = 1-7, l = \mathrm{s-i}$	519 966	224 306	326 933
		Higher-order correlation (Estimation of TQ)				
$\{2s^2\,2p^3 3s\}$	$\{2s^2 2p^4\}$	4SDV	$n = 2-4, l = \mathrm{s-f}$	3542	1267	1658
$\{2s^2\,2p^3 3s\}$	$\{2s^2 2p^4\}$	4SDTQV	$n = 2-4, l = \mathrm{s-f}$	121 052	61 834	86 051

of the electromagnetic operator [36],

$$S = |\langle \Psi(\Gamma P J) \| T \| \Psi(\Gamma' P' J') \rangle|^2, \tag{4}$$

where T is the transition operator [36]. Two forms of the transition operator for electric dipole ($E1$) transitions are the Babushkin and Coulomb gauges [37], which correspond to the length (len) and velocity (vel) gauges in the nonrelativistic limit [35]. Under these two gauges the line strength takes a form [32,36,38],

$$S^{\mathrm{len}} \approx \left| \left\langle \Psi(\Gamma P J) \left\| \sum_i^N r_i \right\| \Psi(\Gamma' P' J') \right\rangle \right|^2, \tag{5}$$

in the length gauge and

$$S^{\mathrm{vel}} \approx \frac{c^4}{\omega^2} \left| \left\langle \Psi(\Gamma P J) \left\| \sum_i^N \alpha_i \right\| \Psi(\Gamma' P' J') \right\rangle \right|^2, \tag{6}$$

in the velocity gauge. N is the total number of electrons.

More accurate transition rates, which we refer to as adjusted transition rates A_{adj}, can be obtained by scaling the calculated transition rates A_{calc} with the ratio of the observed ω_{obs} and calculated ω_{calc} transition energies to compensate for some of the neglected correlation effects. The energy ratio is denoted by $r = \frac{\omega_{\mathrm{obs}}}{\omega_{\mathrm{calc}}}$ (or $= \frac{\lambda_{\mathrm{calc}}}{\lambda_{\mathrm{obs}}}$) where ω_{obs} is cited from the Atomic Spectra Database (ASD) of the National Institute of Standards and Technology (NIST) [17]. Using it for the length gauge, we have

$$S^{\mathrm{len}}_{(\mathrm{adj})} = S^{\mathrm{len}}_{(\mathrm{calc})} \quad \text{and} \quad A^{\mathrm{len}}_{(\mathrm{adj})} = r^m A^{\mathrm{len}}_{(\mathrm{calc})}, \tag{7}$$

where $m = 3$ for $E1$ or $M1$ transitions and m=5 for $E2$ or $M2$ transitions [23]. For the velocity gauge [36], the case changes to be

$$S^{\mathrm{vel}}_{(\mathrm{adj})} = \frac{1}{r^2} S^{\mathrm{vel}}_{(\mathrm{calc})} \quad \text{and} \quad A^{\mathrm{vel}}_{(\mathrm{adj})} = r A^{\mathrm{vel}}_{(\mathrm{calc})}. \tag{8}$$

The impact for A, affected by this scaling correction, obviously is larger in the case of extremely small ω (or very large λ) [39]. A biorthogonal transformation technique is needed so that standard Racah algebra can be used for evaluating transition matrix elements between states with different orthonormal orbital sets [40]. The GRASP2K package was used for all the calculations [41].

B. Computational model

The computational procedures are summarized in Table I. The reference configurations for the odd and even parity states are taken as $\{2s^2\,2p^3 3s\}$ and $\{2s^2 2p^4\}$, respectively. The orbitals of these configurations are treated as occupied orbitals. The CSFs were formed from all configurations that could be obtained by single (S) and double (D) substitutions of the occupied orbitals. The active sets for the odd and even parity states were extended layer by layer so as to be able to monitor the convergence, and systematically enlarged to include orbitals with principal quantum numbers $n = 2$–8, and orbital quantum numbers $l = 0$–5 (i.e., angular symmetries s, p, d, f, g, h). Here, except for the occupied orbitals, others are treated as correlation orbitals. For the SCF calculations, the $1s^2$ core is kept closed, and the generated CSF expansions account for

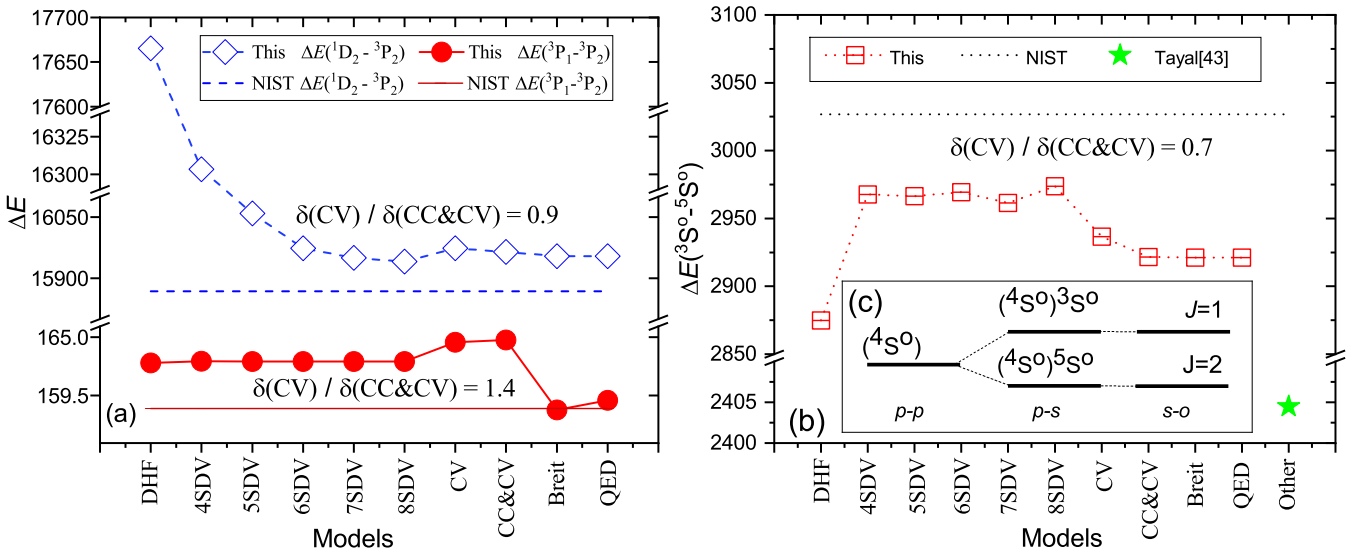

FIG. 1. The energy difference ΔE (cm^{-1}) of $2p^4$ and $2p^3 3s$ in different correlation models. (a) The $\Delta E(^1D_2–^3P_2)$ and $\Delta E(^3P_1–^3P_2)$ in $2p^4$. (b) $\Delta E(^3S^\circ_1–^5S^\circ_2)$ in $2p^3 3s$. (c) Schematic illustration of the development of the separation between $^3S^\circ$ and $^5S^\circ$ in the $p^3 s$ configuration, where the p-p electron interaction produces three terms ($^2P^\circ$), ($^2D^\circ$), and ($^4S^\circ$) of a p^3 subconfiguration. Here, for the latter $p^3(^4S^\circ)$, the p-s interaction produces further separation between the final terms $^3S^\circ$ and $^5S^\circ$. The designation $(^{2S_1+1}L^\circ)^{2S+1}T^\circ$ means that $(^{2S_1+1}L^\circ)$ is the parent of the final term $^{2S+1}T^\circ$ [16]. s-o denotes the small spin-orbit effect. $\frac{\delta_{CV}}{\delta_{CC\&CV}}$ is the influence ratio of CV and CC&CV.

valence (V) correlation. We denote the computational model above by nSDV. In the successive layer calculations, the wave functions optimized in the previous layers were kept frozen, and only the newly added ones were optimized.

The core-valence (CV) and core-core (CC) correlation effects were accounted for in RCI calculations [41] by allowing, respectively, S and D substitutions also from the $1s^2$ core. The corresponding computational model applied to the largest orbital set is denoted CV or CC&CV. It is known that the Breit interaction is important for intercombination transitions, and this interaction along with QED effects was also included in RCI for the largest orbital sets. Once the ASFs have been obtained, the atomic parameters such as S and A can be calculated.

Because of large discrepancies of approximately 400% in the lifetime calculations [11,19,22,23], we also performed other systematic calculations to evaluate accuracy. CASE-II and III are used to change the set of multireference configurations (SMC). Additional calculations were made to estimate the effect of the higher-order correlation with the aid of triple and quadruple (TQ) substitutions. Since the QED effect is minor, we mainly consider the differences in the computed properties in terms of electron correlation and Breit interaction, which are discussed in the following sections.

III. RESULTS AND DISCUSSION

A. Energy levels

The valence correlation effect plays a major role in the optimization of energy levels [42]. Figures 1(a) and 1(b) present the level differences (ΔE) within the $2p^4$ and $2p^3 3s$ configurations in different correlation models. $\Delta E(^1D_2–^3P_2)$ and $\Delta E(^3S^\circ_1–^5S^\circ_2)$ are changed by approximately 1400 and 100 cm^{-1}, respectively, in the 4SDV models compared to DHF. $\Delta E(^3P_1–^3P_2)$ is an exception with small changes. A rare case should be paid much attention, for the level differences with regard to $^5S^\circ_2$, the electron correlation of 8SDV model has certain influence, although its effect rarely appears in the calculations of the normal triplet or singlet states, e.g., that of $^3P_{1,2}$ and $^1D_2$.

The core-core (CC) and core-valence (CV) correlations have certain influences on the energy difference, which can be expressed as

$$\delta_X = \frac{100 \times |\Delta E_X - \Delta E_{8SDV}|}{\max(\Delta E_X, \Delta E_{8SDV})}\%, X = \text{CV, CC\&CV}. \quad (9)$$

Figure 1 shows that the largest δ_X corresponds to the $\Delta E(^3S^\circ_1–^5S^\circ_2)$ of $2p^3 3s$ configuration. Figure 1(c) illustrates the separation between $^3S^\circ$ and $^5S^\circ$, which is produced by the p-s electron interaction. Here, $\delta_{CC\&CV}$ is approximately 2%. In addition, to understand how much the core correlation affects the separation between $^3S^\circ$ and $^5S^\circ$ in other $p^3 s$ configurations, we selected the $2p^3 2s$ configuration of N II, and the MCDHF and MCHF calculations are listed in Table II. It indicates that the effects of the CC&CV correlation change the separation by 531 cm^{-1}. These influences, emerging both in O I and in N II, indicate that the precise calculation of the separation between $^3S^\circ$ and $^5S^\circ$ in the $p^3 s$ configuration is inseparable from the consideration of core correlation. Tayal's MCHF calculation of O I has a large discrepancy of approximately 623 cm^{-1} with the reference value from the NIST atomic spectra database [17] due to the neglected influences of core correlation [Fig. 1(b) or Table II] [43].

To determine the contribution of the CC and CV effects, we use the influence ratio of CV and CC&CV, i.e., $\frac{\delta_{CV}}{\delta_{CC\&CV}}$. Figure 1 shows that the $\frac{\delta_{CV}}{\delta_{CC\&CV}}$ of $\Delta E(^3S^\circ_1–^5S^\circ_2)$ equals 0.7, which is the smallest compared with $\Delta E(^1D_2–^3P_2)$ and $\Delta E(^3P_1–^3P_2)$.

TABLE II. The influences of the core correlation and relativistic effect on the separation between $^3S^\circ$ and $^5S^\circ$ in the $2p^3n_2s$ configurations, where n_2 is equal to 3 and 2 for O I and N II, respectively. The integer form is adopted for all the data.

	$\Delta E(^3S^\circ\text{-}^5S^\circ)$ of $2p^3n_2s$ (n_2=3 or 2) (cm^{-1})			
	O I ($2p^33s$)		N II ($2p^32s$ or $2s2p^3$)	
Models	ΔE	$\lvert\Delta E-\Delta E_{\rm NIST}\rvert$	ΔE	$\lvert\Delta E-\Delta E_{\rm NIST}\rvert$
MCDHF calculations in this team				
8SDV[a]	2974	53		
7SDV[b]			109 919	1577
nSDV + CC&CV [a,b]	2922	105	109 388	1046
MCHF calculations by Tayal				
Neglected $1s^2$[c]	2404	623		
CV[d]			109 571	1229
Nonrelativistic calculation				
OP[e]	3042	15	112 706	4364
Other calculation				
Zeippen[f]	1740	1287		
Experiment				
NIST[g]	3027	0	108 342	0

[a]This work.
[b]Shen *et al.* 2016 [24].
[c]Tayal 2009 [43].
[d]Tayal 2011 [44].
[e]Opacity Project [45].
[f]Zeippen *et al.* 1977 [11].
[g]NIST 2019 [17].

This indicates that both CC and CV correlations have certain influences on the separation between $^3S^\circ$ and $^5S^\circ$.

Furthermore, it should be stressed that the relativistic effect contributes differently to the separation between $^3S^\circ$ and $^5S^\circ$ in the different $n_1p^3n_2s$ configurations, e.g., those of $2p^33s$ in O I and $2p^32s$ in N II. Table II also lists a nonrelativistic calculation reported by the Opacity Project (OP). The table reveals that the difference between the OP and NIST values is 15 cm^{-1} in O I but increases to 4364 cm^{-1} in N II. However, our relativistic calculations agree with NIST to 53 cm^{-1} in O I and 1577 cm^{-1} in N II. These results imply that when the s electron moves from a peripheral orbital closer to the core, the relativistic effect manifests itself in increased level separation.

B. Transition rates

The line strengths S and radiative rates A of transitions from the $2p^33s\ ^5S^\circ_2$ to the levels of the ground term $2p^4\ ^3P$ and to ^1D in the different models and the length gauge are listed in Table III. 4SDV almost doubles the results of DHF. The effects of the CV and CC&CV correlations are small except for the case of $^1D_2$-$^5S^\circ_2$ with the wavelength by λ172.711 nm. Introduction of the Breit interaction changes the data of $^3P_2$–$^5S^\circ_2$ (or λ135.560 nm) and $^3P_1$–$^5S^\circ_2$ (or λ135.851 nm) by about 18% and 24%, respectively. However, this effect dramatically changes the rate of λ172.711 nm by approximately 6 orders of magnitude. To avoid the rate errors produced by the calculated transition energy, the adjusted rate is cited [23]. The final results together with the uncertainties estimated in Sec. III F are listed in Table III.

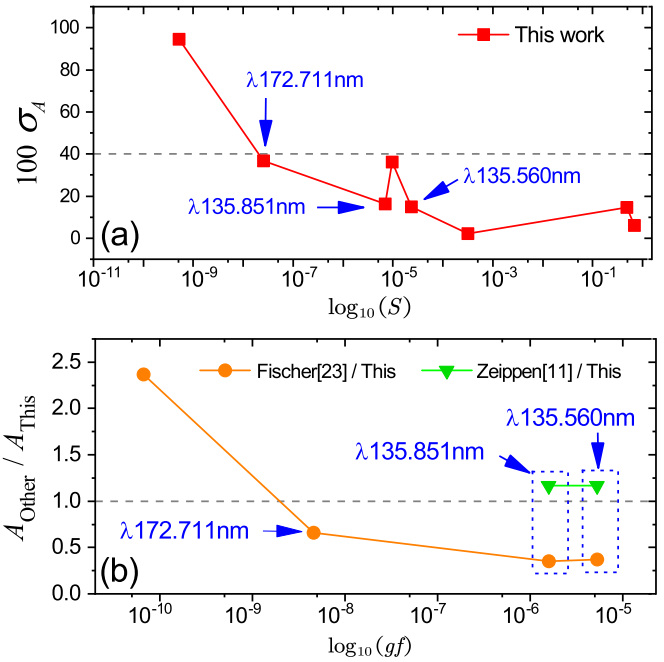

FIG. 2. (a) The discrepancies (σ_A) of intercombination $2p^4$–$2p^33s$ transition rates between the length and velocity gauges. (b) The rate ratio of other calculations and the present work in the length gauge. gf is the weighted oscillator strength. The three lines from $2p^33s\ ^5S^\circ_2$ are marked by λ172.711 nm, λ135.851 nm, and λ135.560 nm. Zeippen *et al.* reported the gf values [11] based on which Meier calculated the corresponding transition rates [10].

The accuracy of A, defined by σ_A, can be evaluated through the agreement between values in the velocity and length gauges [46],

$$\sigma_A = \frac{100 \times |A_{\rm vel} - A_{\rm len}|}{\max(A_{\rm vel}, A_{\rm len})}\%. \tag{10}$$

The values of σ_A for spin-forbidden $2p^4$–$2p^33s$ transitions are presented in Fig. 2(a). As one can see, most of them decrease with increasing line strength and are lower than 40%. The σ_A values of λ172.711 nm, λ135.851 nm, and λ135.560 nm are 37%, 16%, and 15%, respectively.

MCHF calculations of Froese Fischer and Tachiev [23] quoted in Table III, including both S and A of λ135.560 and 135.851 nm in the length gauge, are all smaller than our results. For 172.711 nm, they are smaller by about 32%, while for the other two transitions they are smaller by about a factor of 3. In Fig. 2(b), we also use the rate ratio $\frac{A_{\rm Fischer}}{A_{\rm This}}$ to illustrate the discrepancies. Froese Fischer also performed an earlier calculation of weighted oscillator strength (gf) from $^5S^\circ_2$ [22]. Her calculations of gf of $^3P_2$–$^5S^\circ_2$, $^3P_1$–$^5S^\circ_2$, and $^1D_2$–$^5S^\circ_2$ yielded, respectively, 1.93×10^{-6}, 5.36×10^{-7}, and 3.87×10^{-9}. Correspondingly, our QED calculations of gf yield 5.28×10^{-6}, 1.58×10^{-6}, and 4.55×10^{-9}. The two MCHF calculations of Froese Fischer differ very little despite the fact that nearly 20 years have been passed between the two efforts [22,23]. Froese Fischer and Tachiev [23] treated

TABLE III. Line strengths (S), transition rates (A), and branching ratio (BR) of $E1$ transitions from $2p^3 3s\ ^5S^\circ_2$ in O I with different computational models in CASE-I. Adjusted is the result rescaled to experimental transition energy. Uncertainty is estimated in Sec. III F. $a[b]$ denotes $a \times 10^b$. The unit of S here and in Tables IV and VII is atomic unit [16]. The S and A data here and in Tables IV and VII are kept to two digits after the decimal point, and BR to three digits.

	S and A of $2p^4$–$2p^3 3s\ ^5S^\circ_2$						
	$^3P_2$–$^5S^\circ_2$ (λ135.560 nm)		$^3P_1$–$^5S^\circ_2$ (λ135.851 nm)		$^1D_2$–$^5S^\circ_2$ (λ172.711 nm)		BR
Models	S	A (s^{-1})	S	A (s^{-1})	S	A (s^{-1})	$\frac{A_{\lambda 135.560\ \mathrm{nm}}}{A_{\lambda 135.851\ \mathrm{nm}}}$
			Valence (in length gauge)				
DHF	1.76[−5]	1.68[3]	5.76[−6]	5.46[2]	3.99[−12]	1.39[−4]	3.079
4SDV	2.63[−5]	3.97[3]	8.58[−6]	1.29[3]	7.13[−13]	5.00[−5]	3.081
5SDV	2.73[−5]	4.19[3]	8.91[−6]	1.36[3]	1.58[−12]	1.14[−4]	3.081
6SDV	2.78[−5]	4.30[3]	9.08[−6]	1.39[3]	1.55[−13]	1.14[−5]	3.082
7SDV	2.81[−5]	4.36[3]	9.19[−6]	1.41[3]	1.64[−15]	1.20[−7]	3.082
8SDV	2.87[−5]	4.44[3]	9.37[−6]	1.44[3]	5.74[−13]	4.23[−5]	3.082
			Core-core (CC), core-valence (CV), and valence (in length gauge)				
CV	2.86[−5]	4.50[3]	9.34[−6]	1.46[3]	6.81[−15]	5.12[−7]	3.082
CC&CV	2.82[−5]	4.69[3]	9.21[−6]	1.52[3]	1.65[−14]	1.33[−6]	3.083
			Breit, QED (in length gauge)				
Breit	2.32[−5]	3.86[3]	6.98[−6]	1.15[3]	2.56[−8]	2.06[0]	3.353
QED	2.34[−5]	3.89[3]	7.02[−6]	1.16[3]	2.57[−8]	2.07[0]	3.352
Adjusted		3.80[3]		1.13[3]		2.02[0]	3.352
			Final results with uncertainties (in length gauge)				
Final	2.34 ± 0.33[−5]	3.80 ± 0.53[3]	7.02 ± 1.05[−6]	1.13 ± 0.17[3]	2.57 ± 1.80[−8]	2.02 ± 1.41	3.352 ± 0.067
			Final results with uncertainties in velocity gauge				
QED	1.99[−5]	3.31[3]	5.87[−6]	9.69[2]	4.06[−8]	3.27[0]	3.414
Adjusted	2.02[−5]	3.29[3]	5.95[−6]	9.62[2]	4.13[−8]	3.25[0]	3.414
Final	2.02 ± 0.28[−5]	3.29 ± 0.46[3]	5.95 ± 0.89[−6]	9.62 ± 1.44[2]	4.13 ± 2.89[−8]	3.25 ± 2.28[0]	3.414 ± 0.068
			Other theories				
MCHF[a]	8.839[−6]	1.438[3]	2.533[−6]	4.094[2]	1.737[−8]	1.367[0]	3.512
Zeippen *et al.*[b]		4.575[3]		1.207[3]			3.790
Garstang[c]		1.30[3]		3.90[2]		2.00[0]	3.333

[a]Froese Fischer and Tachiev in length gauge [23].
[b]Meier [10] calculated the transition rates based on gf values of Zeippen *et al.* [11].
[c]Garstang [19].

$1s^2$ as a common core and only considered correlation among the remaining electrons, and some relativistic corrections in their work have also been neglected. Another possible reason for discrepancies between our calculations and MCHF can be poorer accuracy of the MCHF wave functions. One can see the detailed analysis in Sec. III G.

Furthermore, the S and A values from $^5S^\circ_2$ in velocity gauge including QED, adjusted, and final results with uncertainties are presented in Table III. We also list the S and A values for the forbidden magnetic quadrupole ($M2$) transitions from $^5S^\circ_2$ in Table IV.

C. Branching ratio

The branching ratio (BR) is necessary for determining the electron densities of many astrophysical plasma environments, e.g., that of the Orion nebula [2], and is defined by

$$\mathrm{BR} = \frac{A(^3P_2 - {}^5S^\circ_2)}{A(^3P_1 - {}^5S^\circ_2)}, \left(\text{or} = \frac{A_{\lambda 135.560\ \mathrm{nm}}}{A_{\lambda 135.851\ \mathrm{nm}}}\right). \tag{11}$$

Because the wavelength difference between the transitions $^3P_2$–$^5S^\circ_2$ and $^3P_1$–$^5S^\circ_2$ is rather small, e.g., 135.851–135.560 nm = 0.291 nm, the errors produced by the wavelengths are reduced in calculations. In this case, the BR value is almost equal to the ratio of the line strengths of $^3P_2$–$^5S^\circ_2$ and $^3P_1$–$^5S^\circ_2$, i.e., $\frac{A(^3P_2 - {}^5S^\circ_2)}{A(^3P_1 - {}^5S^\circ_2)} \approx \frac{S(^3P_2 - {}^5S^\circ_2)}{S(^3P_1 - {}^5S^\circ_2)}$.

In order to see BR's properties, the trends of ratios of the S value of each successive calculational layer to the result of the largest one, $S_{8\mathrm{SDV}}$, namely $\frac{S}{S_{8\mathrm{SDV}}}$, are depicted in Fig. 3 in the length and velocity gauges for each transition. It illustrates two observations "Coincidence" and "Separation." The "Coincidence" shows that the calculation trends of $\frac{S}{S_{8\mathrm{SDV}}}$ from DHF to the CC&CV model are the same for both transitions in length (or velocity) gauge. This reflects a fact that the BR calculations remain stable in different electron correlation models. We infer that it is a peculiar intrinsic property of these calculations that leads to a truly useful result for plasma diagnostics and other applications, e.g., using the "Coincidence" BR value [11], the transition rates $A(^3P_2$–$^5S^\circ_2)$ and $A(^3P_1$–$^5S^\circ_2)$ could be derived from the accurately known recommended

TABLE IV. Line strengths and transition rates for magnetic quadrupole ($M2$) transitions from the $2p^3 3s\ ^5S^\circ_2$ level of O I.

Lower	States	Upper	State	Type	S	$A\ (s^{-1})$	
						MCDHF(QED)	Adjusted
$2p^4$	$^3P_0$	$2p^3 3s$	$^5S^\circ_2$	$M2$	3.45[0]	2.29[−3]	2.21[−3]
	$^1S_0$		$^5S^\circ_2$	$M2$	9.41[−10]	2.93[−14]	2.86[−14]
	$^3P_1$		$^5S^\circ_2$	$M2$	7.78[0]	5.20[−3]	5.01[−3]
	$^3P_2$		$^5S^\circ_2$	$M2$	6.08[0]	4.11[−3]	3.96[−3]
	$^1D_2$		$^5S^\circ_2$	$M2$	8.80[−5]	1.78[−8]	1.71[−8]

lifetime [27]. The BR values in different models in length gauge are also listed in Table III.

On the other hand, adding the Breit interaction makes some differences for the two transitions because of the different sensitivity of the line strengths to this effect, i.e., "Separation" in Fig. 3. This affects the calculations of BR. Setting length calculation as an example, the Breit interaction changes the line strengths (or rates) of λ135.560 and 135.851 nm by 18% and 24%, respectively. These different influences, nearly 6% between two decays, cause a large change of BR from 3.083 to 3.353. It signifies that the decays of two channels $^3P_2$–$^5S^\circ_2$ and $^3P_1$–$^5S^\circ_2$ have different sensitivity to the effects of the magnetic interaction and the lowest-order retardation correction to the electrostatic interaction [34], e.g., the result 3.790 of Zeippen *et al.* [11] is larger than our length result by about 12% in Table III because the calculation of Ref. [11] neglected some relativistic effects. In the present work, as shown in Table III, the final BR results in length and velocity gauges including their accuracies evaluated in Sec. III F, respectively, are 3.352 ± 0.067 and 3.414 ± 0.068. The average of the length and velocity results, 3.383 ± 0.068, can be as the final recommended value because the uncertainties given in Table III for both forms of BR are nearly the same, and the values agree well with each other.

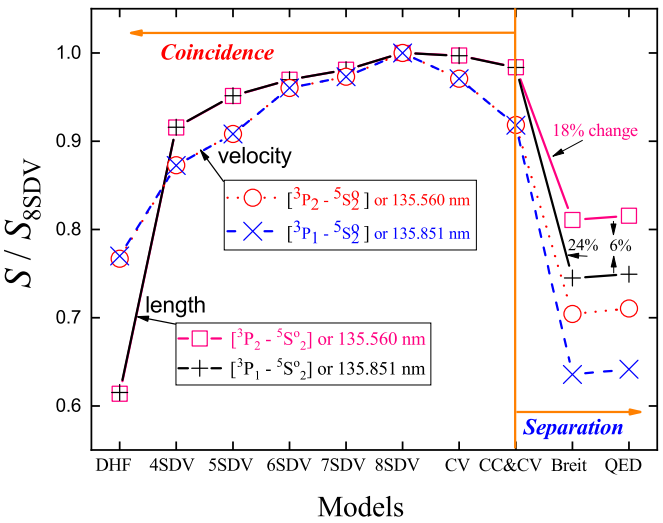

FIG. 3. The calculation trends of $\frac{S}{S_{8SDV}}$ of $2p^4\ ^3P_{1,2}$–$2p^3 3s\ ^5S^\circ_2$ in the length and velocity gauges in the different computational models. "Coincidence" is observed among the DHF through CC&CV models, and "Separation" is produced by the Breit interaction. The data in the length gauge are also listed in Table III.

D. Branching fraction

The branching fractions k and k_1 for $^3P_2 - {}^5S^\circ_2$ and $^3P_1 - {}^5S^\circ_2$ can be given by

$$\begin{cases} k = \frac{A(^3P_2 - {}^5S^\circ_2)}{A(^3P_2 - {}^5S^\circ_2)+A(^3P_1 - {}^5S^\circ_2)+A(^1D_2 - {}^5S^\circ_2)} \\ k_1 = \frac{A(^3P_1 - {}^5S^\circ_2)}{A(^3P_2 - {}^5S^\circ_2)+A(^3P_1 - {}^5S^\circ_2)+A(^1D_2 - {}^5S^\circ_2)}. \end{cases} \quad (12)$$

If combined with another branching ratio of $^5S^\circ_2$, defined by $\mathrm{BR}_1 = \frac{A(^1D_2 - {}^5S^\circ_2)}{A(^3P_2 - {}^5S^\circ_2)}$, the relationship between the branching fractions and two branching ratios BR and BR_1 can be arrived at

$$\begin{cases} k = \frac{1}{1+\frac{1}{\mathrm{BR}}+\mathrm{BR}_1} \\ k_1 = \frac{1}{1+\mathrm{BR}\times(1+\mathrm{BR}_1)}. \end{cases} \quad (13)$$

Although the uncertainties in the A values given in Table III are relatively large, changes in $A(^3P_2 - {}^5S^\circ_2)$ and $A(^3P_1 - {}^5S^\circ_2)$ among different calculations are found to be strongly correlated, so that the changes in BR are relatively small. Thus, Eq. (13) can be used to estimate the uncertainty of the branching fraction, which is dominated by the uncertainty of BR owing to the very small size of BR_1 (5×10^{-4} in the length form and 1×10^{-3} in the velocity one).

Here, the k and k_1 values in the length and velocity gauges are listed in Table V where although both BR values agree with each other, the velocity form may be preferred because of the slightly smaller uncertainty, as shown in Table VII. In the present work, the straight arithmetic mean value, $k = 0.7714$ (or $k_1 = 0.2280$), with an uncertainty of 0.0035 for both are recommended, because the uncertainties are nearly the same, and the uncertainty is not reduced by averaging as the length and velocity form values are strongly intercorrelated. Hence, the obtained value of k closely agrees with a range of Zeippen *et al.* [11], 0.77–0.78, and with the result of Ref. [23], $k = 0.7778$, while an earlier data of Garstang [19] yield $k = 0.7683$. And $k_1 = 0.2280$ is also in accordance with 0.2215 deduced from the data of Ref. [23].

The direct application of the branching fraction is to extrapolate the rate below when combined with the recommended lifetime [27],

$$\begin{cases} A(^3P_2 - {}^5S^\circ_2) = k \times 1/\tau(^5S^\circ_2) \\ A(^3P_1 - {}^5S^\circ_2) = k_1 \times 1/\tau(^5S^\circ_2). \end{cases} \quad (14)$$

Table V also lists the extrapolated rates of $^3P_2 - {}^5S^\circ_2$ and $^3P_1 - {}^5S^\circ_2$, for which the recommended lifetime $180 \pm 5\ \mu$s [a.k.a. 180(5) μs] [27] is cited, seeing Sec. III E. It shows that

TABLE V. The branching fractions (k & k_1) of $^3P_2 - {}^5S_2^\circ$ and $^3P_1 - {}^5S_2^\circ$, and their extrapolated transition rates using the recommended lifetime 180 ± 5 μs [a.k.a. 180(5) μs] [27]. 4279 is inferred using $\frac{10^6 k}{3}(\frac{1}{\tau_1}+\frac{1}{\tau_2}+\frac{1}{\tau_3})$ and (120) is the maximum discrepancy between 4279 and other $\frac{10^6 k}{\tau_i}$ where τ_i adopts 180, 175, 185 for $i = 1, 2, 3$. Mean value denotes the straight arithmetic mean value in the length (len) and velocity (vel) gauges. aE-b denotes $a \times 10^{-b}$.

	Branching ratios		Branching fractions and the extrapolated rates			
			$^3P_2 - {}^5S_2^\circ$		$^3P_1 - {}^5S_2^\circ$	
Type	BR	BR_1	k	$A(k)$	k_1	$A(k_1)$
			This work			
len	3.352(67)	5.32×10^{-4}	0.7699(35)	4279(120)	0.2297(35)	1277(36)
vel	3.414(68)	9.88×10^{-4}	0.7729(35)	4296(120)	0.2264(35)	1258(35)
Mean value			0.7714(35)	4288(120)	0.2280(35)	1267(36)
			Some extrapolations			
MCHF[a]	3.512	9.51×10^{-4}	0.7778	4323(121)	0.2215	1231(35)
Garstang[b]	3.333	1.54×10^{-3}	0.7683	4271(120)	0.2305	1281(36)
			Others			
Zeippen *et al.*[c]			0.775(5)	4308(121)		
Wiese *et al.*[d]				4200(420)		1360(136)

[a]Reference [23].
[b]Reference [19].
[c]Reference [11].
[d]Refs. [17,27].

the mean result for k yields $A(^3P_2 - {}^5S_2^\circ) = 4288(120)$ s^{-1}, which coincides with 4308(121) s^{-1}, derived from an average value of 0.77 and 0.78 of Zeippen *et al.* [11], i.e., 0.775(5). The uncertainty is slightly reduced and is entirely dominated by the uncertainty of the lifetime. The relative uncertainty of $A(^3P_2 - {}^5S_2^\circ)$ is 2.8%, which is more than a factor of three smaller than the uncertainty of the value presently recommended by NIST [17], 4200(420) s^{-1} [27]. In addition, the mean value of k_1 yields $A(^3P_1 - {}^5S_2^\circ) = 1267(36)$ s^{-1}, which has a similar relative uncertainty, also a factor of three more accurate than the presently recommended NIST value of 1360(136) s^{-1} [17,27].

E. Lifetime

The lifetimes τ of $^5S_2^\circ$ in different computational models are illustrated in Fig. 4, where the data in the length and velocity gauges are presented. 4SDV reduces the DHF value by a factor of nearly two, and the Breit interaction leads to another large change. Here, we also list the lifetimes of CASE-II and III in the length and velocity gauges, which consider the effect of the Breit interaction rather than QED due to the minor size of the latter. The error bars in Fig. 4 show the uncertainties, which are calculated using the data of CASE-II and III, along with the recommended data. The calculated lifetimes of the velocity and length gauges are 235 ± 35 μs and 202 ± 30 μs, respectively. For the convenience of reference, we also list the data of Fig. 4 in Table VI, where the results of other theoretical and experimental studies are also listed with associated uncertainties.

Upon comparing other theoretical lifetimes with the present work, a good agreement is found with the calculations of Nicolaides [20] and Biémont and Zeippen [21]. However, some large discrepancies are still identified with the results of Garstang [19], Froese Fischer [22,23], and Zeippen *et al.* [11]. For example, inspection of Fig. 4 shows that the discrepancies of calculated lifetimes are larger than 325 μs. The largest discrepancy exceeding 400% is between Garstang [19] and Zeippen *et al.* [11]. Garstang has performed a nonrelativistic

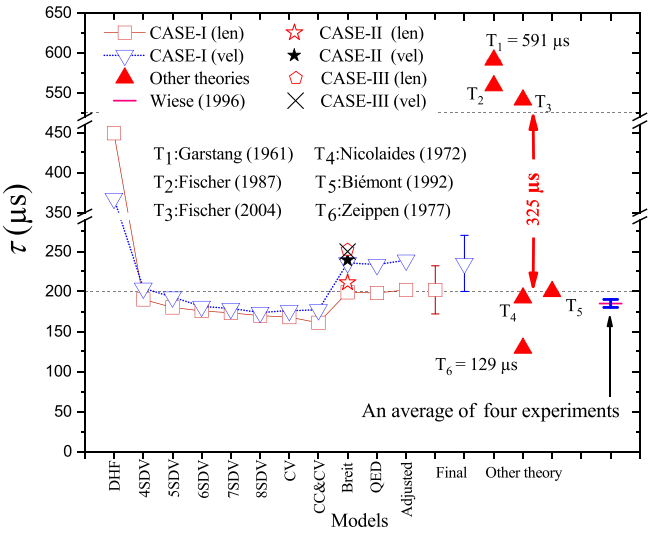

FIG. 4. Radiative lifetimes (τ) of $2p^3 3s\ ^5S_2^\circ$ (μs) in the length (len) and velocity (vel) gauges of CASE-I versus increasing level of electron correlation and other corrections. Final denotes the final result together with the estimated uncertainty marked using an error bar. T_1–T_6 denote six theoretical calculations, where large discrepancy between T_p (p = 1,2,3) and T_q (q=4,5,6) is about 325 μs. Wiese *et al.* [27] gave an average of four different experiments made by other researchers [1,29–31]. The length of the error bar indicates the size of the uncertainty. Some data are also listed in Table VI.

TABLE VI. Radiative lifetimes (τ) of $2p^3 3s\ ^5S_2^\circ$ (μs) in the velocity (vel) and length (len) gauges. Wiese *et al.* [27] gave an average of four different experiments made by other researchers [1,29–31]. All data on lifetimes including that of Table VII adopt an integer form.

		τ (μs)	
Models	Methods	vel	len
	CASE-I		
Breit		236	199
QED		234	198
Adjusted		235	202
	CASE II and III		
CASE-II (Breit)		239	211
CASE-III (Breit)		250	252
	Final results with uncertainties		
Final		235 ± 35	202 ± 30
	Other theories		
Garstang (1961)[a]			591
Nicolaides (1972)[b]		192	
Zeippen *et al.* (1977)[c]	SM + ID		129
Froese Fischer (1987)[d]	MCHF		559
Biémont and Zeippen (1992)[e]	SUPERSTRUCTURE		200
Froese Fischer (2004)[f]	MCHF		541
	Other		
Wiese *et al.* (1996)[g]	TOF		180 ± 5

[a]Reference [19].
[b]Reference [20].
[c]Reference [11].
[d]Deduced Froese Fischer's gf values [22] using experimental wavelengths.
[e]Reference [21].
[f]Reference [23].
[g]Reference [27].

Hartree-Fock calculation [19]. This led to lower rates and a longer lifetime, e.g., $A_{135.6\,\mathrm{nm}} = 1300\ \mathrm{s}^{-1}$ and $\tau = 591\ \mu$s. On the other hand, a somewhat more complicated calculation carried out by Zeippen *et al.*, attained a very small lifetime, i.e., 129 μs [11]. Since the energy difference between $^3S_1^\circ$ and $^5S_2^\circ$ calculated by Zeippen *et al.* [11] is 1740 cm^{-1}, which differs from the NIST experimental data by about 42%, as indicated in Table II, we conclude that their wave function of the upper state was inaccurate. We ascribe the errors in these two calculations [11,19] to some neglected electron correlation and relativistic effects.

The measurements of lifetimes of the $^5S_2^\circ$ level, using the time-of-flight (TOF) technique, lead to values in the range of 170–190 μs [1,29–31]. To obtain the currently recommended value, Wiese *et al.* [27] selected the arithmetic average of these four measurements of lifetimes [1,29–31], in which these results fall within a narrow band of only 5%. Thus, they recommended the average experimental value of $180 \pm 5\ \mu$s [27], which agrees with our calculation in the length gauge, but is more accurate by a factor of eight. Morton [28] also adopted the transition rates derived by Wiese *et al.* [27] from the above experimental lifetime and theoretical branching fractions of Biémont and Zeippen [21].

F. Evaluation of the accuracy

Because of the large errors of up to 400% in some lifetime calculations of $^5S_2^\circ$ in O I [11,19,22,23], it is desirable to examine the reasons of errors, determine the appropriate solutions, and report accurate atomic data. By changing the set of multireference configurations (SMC), two systematic calculations CASE-II and III were also performed. Their Breit results for S, BR, and τ in the length and velocity gauges are listed in Table VII together with the Breit calculations in CASE-I. The results are adjusted and show that all the lifetimes are smaller or equal to 244 μs under the models of CASE-I, II, and III.

The rate uncertainty arises from the residual correlation effects, some of which are produced by changing the SMC. Here, in the velocity (vel) and length (len) gauges, the agreements between the respective Breit calculations of the physical quantities (Q) are cited, and the maximum disagreement in the CASE-I, II, and III is defined as the error of SMC (ξ_{SMC}), namely,

$$\begin{cases} \xi_X = \dfrac{100 \times |Q_{\mathrm{vel}} - Q_{\mathrm{len}}|}{\max(Q_{\mathrm{vel}}, Q_{\mathrm{len}})}\%, X = I, II, III; Q = S, \mathrm{BR}, \tau; \\ \xi_{\mathrm{SMC}} = \max(\xi_I, \xi_{II}, \xi_{III}). \end{cases} \quad (15)$$

Table VII shows that the ξ_{SMC} values for $S(^3P_2 - {}^5S_2^\circ)$, $S(^3P_1 - {}^5S_2^\circ)$, $S(^1D_2 - {}^5S_2^\circ)$, BR, and τ values of $^5S_2^\circ$ in O I are 14%, 15%, 38%, 2%, and 14%, respectively.

Meanwhile, the omitted higher-order correlation effects are estimated by

$$\xi_{\mathrm{TQ}} = \frac{100 \times |Q_{\mathrm{4SDTQV}} - Q_{\mathrm{4SDV}}|}{\max(Q_{\mathrm{4SDTQV}}, Q_{\mathrm{4SDV}})}\%, Q = S, \mathrm{BR}, \tau. \quad (16)$$

TABLE VII. The Breit calculations of S, BR, and τ of $^5S_2^\circ$ in CASE-I, II, and III, as well as the estimated uncertainties and the differences between velocity and length gauges [Diff.(v,l)]. ξ stands for uncertainty that combines $\xi_{\rm SMC}$ and $\xi_{\rm TQ}$. SMC denotes the sets of multireference configurations, which were varied to estimate the effect of different correlation models. TQ represents the triple and quadruple substitutions that are used for considering some higher-order electron correlation effects. $\zeta^{\rm vel}$ (or $\zeta^{\rm len}$) is the discrepancy among the calculations of S, BR, τ in the velocity (or length) gauge in CASE-I, II, and III. The branching ratios and the lifetimes are calculated using the adjusted transition rates. All the computational models are shown in Table I.

		Adjusted Breit calculations in three cases						Evaluated accuracy			Diff.(v,l)	
		CASE-I		CASE-II		CASE-III		$\xi_{\rm SMC}$	$\xi_{\rm TQ}$	$\sqrt{\xi_{\rm SMC}^2+\xi_{\rm TQ}^2}$		
Models	Types	vel	len	vel	len	vel	len	$\max(\xi_I,\xi_{II},\xi_{III})$	Higher-order	Final accuracy	$\zeta^{\rm vel}$	$\zeta^{\rm len}$
						Line strengths						
$^3P_2$-$^5S_2^\circ$	S	2.00[−5]	2.32[−5]	1.98[−5]	2.22[−5]	1.95[−5]	2.04[−5]	14%	0%	14%	3%	12%
$^3P_1$-$^5S_2^\circ$	S	5.90[−6]	6.98[−6]	5.83[−6]	6.65[−6]	5.75[−6]	6.03[−6]	15%	0%	15%	3%	14%
$^1D_2$-$^5S_2^\circ$	S	4.12[−8]	2.56[−8]	4.11[−8]	2.84[−8]	3.61[−8]	4.64[−8]	38%	59%	70%	12%	45%
						Branching ratios						
$\frac{A_{(^3P_2-^5S_2^\circ)}}{A_{(^3P_1-^5S_2^\circ)}}$	BR	3.417	3.353	3.418	3.363	3.411	3.412	2%	0%	2%	0%	2%
						Lifetimes						
$^5S_2^\circ$	$\tau(\mu s)$	237	204	240	213	244	232	14%	4%	15%	3%	12%

Here, $Q_{\rm 4SDV}$ are the quantities of the 4SDV model, and $Q_{\rm 4SDVTQ}$ are those of a model where triple and quadruple (TQ) substitutions are also allowed in the {2s–4s, 2p–4p, 3d–4d, 4f} active set. Table VII lists the $\xi_{\rm TQ}$ values as 0%, 0%, 59%, 0%, and 4%, where the largest error corresponds to $S(^1D_2-{}^5S_2^\circ)$.

In the present work, the final adopted uncertainty is the sum in quadrature of $\xi_{\rm SMC}$ and $\xi_{\rm TQ}$, i.e., $\sqrt{\xi_{\rm SMC}^2+\xi_{\rm TQ}^2}$. These uncertainties are given as 14%, 15%, 70%, 2%, and 15% in Table VII, where again, the largest uncertainty corresponds to the weakest transition ($^1D_2$–$^5S_2^\circ$). All values of $\xi_{\rm SMC}$ are greater than $\xi_{\rm TQ}$, except for S of $^1D_2$–$^5S_2^\circ$. The latter implies that the higher-order correlation effect becomes important in this weak decay.

G. Calculation of the differences in the length and velocity gauges

Nicolaides [20] mentioned that the transition rates in length and velocity gauges are in excellent agreement in C I because its active electron does not change shells. However, in the O I case where the active electron changes the principal quantum number, the two gauges are in poor agreement. He presented a viewpoint that the velocity operator is to be preferred when the wave function of the upper state is not accurate enough, and only reported a velocity-form lifetime of 192 μs [20]. Zeippen *et al.* [11] criticized Nicolaides' velocity result and only gave a length-form value of 129 μs. However, this value, nearly the smallest one among the available data, is unreliable because the wave function of Ref. [11] for $^5S_2^\circ$ was inaccurate, as shown in Sec. III E. Hence, it is informative to compare the calculations of the length and velocity gauges.

Since the sets of multireference configurations (SMC) were gradually expanded from CASE-I to III, the discrepancies (ζ) of the velocity physical quantities (Q) among the three cases, or that of the length Q among these cases, are selected. Here, the maximum one in every gauge can be used to analyze the difference of calculations, respectively, in the velocity and length gauges:

$$\begin{cases} \zeta^Y_{(i,j)} = \frac{100\times|Q_i-Q_j|}{\max(Q_i,Q_j)}\%, \ i \ or \ j = I, II, III; \\ Q = S, \mathrm{BR}, \tau; \\ \zeta^Y = \max\left(\zeta^Y_{(I,II)}, \zeta^Y_{(I,III)}, \zeta^Y_{(II,III)}\right), \\ Y = \mathrm{vel \ or \ len}. \end{cases} \tag{17}$$

As seen in Table VII, the uncertainties in the length gauge ($\zeta^{\rm len}$) are much larger than those in the velocity one ($\zeta^{\rm vel}$). This implies that, for the spin-forbidden channels of $^5S_2^\circ$ with small decay rates, calculation of the transition operator in the length gauge becomes much more sensitive to electron correlation effects than in the velocity gauge, if the transition operator applies to the wave function that is not accurate enough. In other words, when accurately calculating the electric dipole matrix element in the length gauge, the requirement for the accuracy of the wave function is very high.

However, due to neglecting the influences of $1s^2$ electrons, it is very difficult to obtain a high precision wave function by a theoretical calculation [22,23,43]. That is probably one of the reasons why Froese Fischer's calculated lifetime, given in the length gauge, is so large, even though the calculations were performed twice [22,23].

IV. CONCLUSIONS

Using the MCDHF method, the line strengths, transition rates, branching ratio, branching fraction, and lifetime of the $^5S_2^\circ$ metastable state in O I were accurately calculated by considering the CC, CV, and valence correlation effects, as well as the Breit interaction and the QED effect. The core correlation effect has a significant influence on the calculated quantities, especially on the separation between $^3S^\circ$ and $^5S^\circ$—produced by the p-s electron interaction—in the p^3s configuration. It is found that the calculations of the branching ratio of $^5S_2^\circ$ remain stable in different electron correlation

models. We infer that it is a peculiar intrinsic property leading to results useful for plasma diagnostics and other applications, e.g., those using the BR value [11]. Improved values of the transition rates $A(^3P_2–^5S_2^\circ)$ and $A(^3P_1–^5S_2^\circ)$ have been derived from the accurately known recommended lifetime [27] and the presently calculated BR. The Breit interaction has a large influence on the radiative decay rates from $^5S_2^\circ$, because the line strengths of $^3P_2–^5S_2^\circ$ (λ135.560 nm) and $^3P_1–^5S_2^\circ$ (λ135.851 nm) are different in sensitivity to this effect. This affects the calculations of the branching ratio and lifetime. The large discrepancies in lifetimes, up to 400% in several theoretical calculations [11,19,22,23], are attributed mainly to some neglected electron correlations and relativistic effects. In addition, by making calculations with various sets of multireference configurations, we find the calculations of electric dipole matrix elements for $^5S_2^\circ$ in the length gauge to be much more sensitive to electron correlation effects than in the velocity gauge. This may also cause significant errors in the calculations of the lifetime of $^5S_2^\circ$ in the length gauge. The present calculations including the estimation of residual electron correlation effects are in fairly good agreement with the recommended data [27] and have potential applications in astrophysics and other related fields, e.g., the diagnosis of ionospheric electron density [5] would lead to better results if substituting their BR result 3.790 [5,10,11] with our recommended 3.383 ± 0.068, an average of the length and velocity results because the uncertainties for both forms of BR are nearly the same.

ACKNOWLEDGMENT

We thank the Natural Science Foundation of Hebei Province (Grant No. A2019109076) for financial support.

[1] N. J. Mason, Meas. Sci. Technol. **1**, 596 (1990).
[2] R. H. Rubin, P. G. Martin, R. J. Dufour, G. J. Ferland, J. A. Baldwin, J. J. Hester, and D. K. Walter, Astrophys. J. **495**, 891 (1998).
[3] K. Haris and A. Kramida, J. Phys. Commun. **1**, 035013 (2017).
[4] G. Wautelet, B. Hubert, J. C. Gérard, and T. J. Immel, J. Geophys. Res. Space Phys. **124**, 7670 (2019).
[5] J. Q. Qin, J. J. Makela, F. Kamalabadi, and R. R. Meier, J. Geophys. Res. Space Phys. **120**, 10116 (2015).
[6] Y. L. Zhang and H. Kil, J. Geophys. Res. **118**, 3584 (2013).
[7] M. L. Hsu, C. H. Lin, R. R. Hsu, J. Y. Liu, L. J. Paxton, H. T. Su, H. F. Tsai, P. K. Rajesh, and C. H. Chen, J. Geophys. Res. Space Phys. **116**, A07313 (2011).
[8] Q. Gan, R. W. Eastes, A. G. Burns, W. B. Wang, L. Y. Qian, S. C. Solomon, M. V. Codrescu, and W. E. McClintock, J. Geophys. Res. Space Phys. **125**, e2020JA027880 (2020).
[9] G. X. Ding, B. Chen, X. X. Zhang, and F. He, J. Atmos. Sol.-Terr. Phys. **199**, 105196 (2020).
[10] R. R. Meier, Space Sci. Rev. **58**, 1 (1991).
[11] C. J. Zeippen, M. J. Seaton, and D. C. Morton, Mon. Not. R. Astron. Soc. **181**, 527 (1977).
[12] B. Ritter, J. C. Gerard, L. Gkouvelis, B. Hubert, S. K. Jain, and N. M. Schneider, J. Geophys. Res. Space Phys. **124**, 4809 (2019).
[13] P. M. Molyneux, J. D. Nichols, N. P. Bannister, E. J. Bunce, J. T. Clarke, S. W. H. Cowley, J. C. Gerard, D. Grodent, S. E. Milan, and C. Paty, J. Geophys. Res. Space Phys. **123**, 3777 (2018).
[14] P. D. Feldman, M. F. A. Hearn, L. M. Feaga, J. L. Bertaux, J. Noonan, J. W. Parker, E. Schindhelm, A. J. Steffl, S. A. Stern, and H. A. Weaver, Astrophys. J. Lett. **825**, L8 (2016).
[15] L. Roth, J. Saur, K. D. Retherford, D. F. Strobel, P. D. Feldman, M. A. McGrath, J. R. Spencer, A. Blöcker, and N. Ivchenko, J. Geophys. Res. Space Phys. **121**, 2143 (2016).
[16] R. D. Cowan, *The Theory of Atomic Structure and Spectra* (University of California Press, Berkeley, 1981).
[17] A. Kramida, Y. Ralchenko, and J. Reader, *Atomic Spectra Database (Ver. 5.7.1)* (NIST ASD Team, National Institute of Standards and Technology, Gaithersburg, 2019); https://physics.nist.gov/asd.
[18] X. Z. Shen, J. Liu, C. C. Sang, and P. Jönsson, Phys. Rev. A **97**, 012510 (2018).
[19] R. H. Garstang, Math. Proc. Cambridge Philos. Soc. **57**, 115 (1961).
[20] C. A. Nicolaides, Chem. Phys. Lett. **17**, 436 (1972).
[21] E. Biémont and C. Zeippen, Astron. Astrophys. **265**, 850 (1992).
[22] C. Froese Fischer, J. Phys. B: At. Mol. Phys. **20**, 1193 (1987).
[23] C. Froese Fischer and G. Tachiev, At. Data Nucl. Data Tables **87**, 1 (2004).
[24] X. Z. Shen, J. Liu, and F. Y. Zhou, Mon. Not. R. Astron. Soc. **462**, 1203 (2016).
[25] J. Liu, X. Z. Shen, K. Wang, and C. C. Sang, J. Chem. Phys. **152**, 204303 (2020).
[26] A. Hibbert, Galaxies **6**, 77 (2018).
[27] W. L. Wiese, J. R. Fuhr, and T. M. Deters, *Atomic Transition Probabilities of Carbon, Nitrogen, and Oxygen – A Critical Data Compilation*, J. Phys. Chem. Ref. Data, Monograph No. 7 (AIP Press, Melville, 1996).
[28] D. C. Morton, Astrophys. J. Suppl. Ser. **149**, 205 (2008).
[29] C. E. Johnson, Phys. Rev. A **5**, 2688 (1972).
[30] W. C. Wells and E. C. Zipf, Phys. Rev. A **9**, 568 (1974).
[31] G. Nowak, W. L. Borst, and J. Fricke, Phys. Rev. A **17**, 1921 (1978).
[32] I. P. Grant, *Relativistic Quantum Theory of Atoms and Molecules: Theory and Computation* (Springer, Berlin/Heidelberg, 2007).
[33] C. Froese Fischer, M. Godefroid, T. Brage, P. Jönsson, and G. Gaigalas, J. Phys. B: At. Mol. Phys. **49**, 182004 (2016).
[34] F. A. Pappia and I. Grant, J. Phys. II **1**, C1-33 (1991).
[35] J. Ekman, M. R. Godefroid, and H. Hartman, Atoms **2**, 215 (2014).
[36] M. Bilal, A. V. Volotka, R. Beerwerth, J. Rothhardt, V. Hilbert, and S. Fritzsche, Phys. Rev. A. **99**, 062511 (2019).
[37] I. P. Grant, J. Phys. B: At. Mol. Phys. **7**, 1458 (1974).
[38] Z. Rudzikas, *Theoretical Atomic Spectroscopy* (Cambridge University Press, Cambridge, 1997).
[39] X. Z. Shen, J. G. Li, P. Jönsson, and J. G. Wang, Astrophys. J. **801**, 129 (2015).

[40] J. Olsen, M. R. Godefroid, P. Jönsson, P. A. Malmqvist, and C. Froese Fischer, Phys. Rev. E **52**, 4499 (1995).
[41] P. Jönsson, G. Gaigalas, J. Bieroń, C. Froese Fischer, and I. P. Grant, Comput. Phys. Commun. **184**, 2197 (2013).
[42] C. C. Sang, Z. B. Chen, Y. Sun, X. Z. Shen, F. Hu, J. Ma, and X. L. Wang, J. Elec. Spec. Rel. Phen. **230**, 26 (2019).
[43] S. S. Tayal, Phys. Scr. **79**, 015303 (2009).
[44] S. S. Tayal, Phys. Rev. A **83**, 012515 (2011).
[45] The Opacity Project Team, *The Opacity Project*, Vol. 1 (Institute of Physics, London, 1995), http://cdsweb.u-strasbg.fr/topbase/topbase.html.
[46] C. Froese Fischer, Phys. Scrip. **T134**, 014019 (2009).